The Journal of Prevention of Alzheimer's Disease 13 (2026) 100501

Contents lists available at ScienceDirect

The Journal of Prevention of Alzheimer's Disease

journal homepage: www.elsevier.com/locate/tjpad

Spatial amyloid–informed multimodal brain age as an early marker of Alzheimer's-related vulnerability and risk stratification

Liang Cui [a,1], Qing-Min Wang [b,1], Zhen Zhang [a], Min Wang [b], You-Yi Tu [a], Jie-Hui Jiang [b], Yi-Hui Guan [c], Yue-Hua Li [d,***], Fang Xie [c,**], Qi-Hao Guo [a,*]

[a] Department of Gerontology, Shanghai Sixth People's Hospital Affiliated to Shanghai Jiao Tong University School of Medicine, 600 Yishan Road, Shanghai, 200233, China
[b] School of Life Sciences, Shanghai University, 99 Shangda Road, Shanghai, 200444, China
[c] Department of Nuclear Medicine & PET Center, Huashan Hospital, Fudan University, 518 East Wuzhong Road, Shanghai, 200040, China
[d] Department of Radiology, Shanghai Sixth People's Hospital Affiliated to Shanghai Jiao Tong University School of Medicine, 600 Yishan Road, Shanghai, 200233, China

ARTICLE INFO

Keywords:
Alzheimer's disease
Brain age gap
Amyloid-beta
Cognitive decline
Plasma biomarkers
Functional connectivity

ABSTRACT

Background: Brain age gap (BAG)—the difference between predicted and chronological age—captures neurobiological aging, but MRI-only models insufficiently reflect Alzheimer's disease (AD) pathology. Whether incorporating regional amyloid-β (Aβ) positron emission tomography (PET) improves sensitivity to early AD processes remains unknown.
Objectives: To develop an amyloid-informed multimodal BAG model and examine its associations with cognition, plasma biomarkers, and functional connectivity across the AD continuum.
Design: Cross-sectional analysis using integrated machine-learning models.
Setting: Chinese Preclinical Alzheimer's Disease Study (CPAS), a cohort recruited from community settings and memory clinics.
Participants: Nine hundred ninety community-dwelling adults spanning normal cognition, subjective cognitive decline (SCD), mild cognitive impairment (MCI), and dementia.
Measurements: Regional Aβ-PET and structural MRI informed BAG estimation. Cognitive tests, plasma biomarkers (p-tau217, p-tau181, neurofilament light [NfL], glial fibrillary acidic protein [GFAP], Aβ42/40), and hippocampus–default mode network (DMN) connectivity from resting-state fMRI were assessed.
Results: Higher BAG was associated with greater odds of SCD, MCI, or dementia across the cohort, with stronger effects in Aβ-positive individuals. BAG explained more cognitive variance than global Aβ burden and was linked to multidomain cognitive deficits. Elevated BAG corresponded to higher p-tau217, p-tau181, NfL, and GFAP and lower Aβ42/40, indicating early biomarker alterations. BAG was also associated with reduced hippocampus–DMN connectivity.
Conclusions: An amyloid-informed multimodal BAG model captures convergent AD-related pathology, biomarker alterations, and cognitive vulnerability beyond amyloid burden alone, supporting its value for individualized risk s2tratification and prevention-focused assessment.

* Corresponding author at: Department of Gerontology, Shanghai Sixth People's Hospital Affiliated to Shanghai Jiao Tong University School of Medicine, 600 Yishan Road, Shanghai, 200233, China.
** Corresponding author at: Department of Nuclear Medicine & PET Center, Huashan Hospital, Fudan University, 518 East Wuzhong Road, Shanghai, 200040, China.
*** Corresponding author at: Department of Radiology, Shanghai Sixth People's Hospital Affiliated to Shanghai Jiao Tong University School of Medicine, 600 Yishan Road, Shanghai, 200233, China.
E-mail addresses: liyuehua312@163.com (Y.-H. Li), fangxie@fudan.edu.cn (F. Xie), qhguo@sjtu.edu.cn (Q.-H. Guo).
[1] Liang Cui and Qing-Min Wang contributed equally to this work.

https://doi.org/10.1016/j.tjpad.2026.100501
Received 20 November 2025; Received in revised form 3 January 2026; Accepted 26 January 2026
Available online 6 February 2026

1. Introduction

Alzheimer's disease (AD) represents a major global health burden [1]. Since AD pathology accumulates years before symptoms, sensitive markers are urgently needed to detect early brain vulnerability and monitor disease progression. Biological brain aging often co-occurs and interacts with AD pathology[2]. In this context, the brain age gap (BAG), defined as the difference between predicted and chronological age, has emerged as a promising biomarker of neurobiological aging; higher BAG values are associated with cognitive decline and neuropathological changes[3,4]. However, how BAG integrates with cognitive performance, plasma biomarkers, and functional connectivity across the Alzheimer's continuum remains unclear. A comprehensive evaluation in a single, deeply phenotyped cohort is essential to clarify its relevance for assessing brain aging in AD.

Building on initial efforts based on structural magnetic resonance imaging (MRI) [5], recent research has turned toward multimodal integration for example using data from MRI, metabolic positron emission tomography (PET), or other modalities, to enhance sensitivity to subtle brain change[6–8]. However, amyloid-beta (Aβ)-PET, the gold-standard imaging modality for detecting amyloid pathology in AD, has remained largely absent from brain age modeling. We propose that integrating Aβ-PET with structural MRI offers a biologically grounded and clinically relevant framework for estimating brain age, as these modalities capture complementary aspects of neurodegeneration and pathology. This integrative approach is particularly well-suited for AD as it unites two core disease markers, amyloid pathology and structural degeneration, in a single aging framework[9].

Rather than relying on global Aβ burden, we propose that characterizing the spatial distribution of Aβ deposition across brain regions may enhance sensitivity to early-stage alterations. Evidence indicates that Aβ deposition follows a spatially selective and gradually progressive trajectory starting in the preclinical stage[10–12]. Our prior findings similarly support the clinical and pathological relevance of regional Aβ signals[13,14], emphasizing the importance of spatial patterning. Furthermore, Aβ-PET may suit brain age modeling due to its established role in detecting AD pathology and its age-related accumulation observed in both normal aging and multiple neurodegenerative diseases [15–17]. Taken together, leveraging the spatial patterns of Aβ-PET alongside structural MRI may allow for more accurate and biologically informative brain age estimates in AD.

In this study, we aimed to construct a multimodal brain age prediction model by combining regional Aβ-PET and structural MRI features. Using a cohort spanning the full AD continuum, we estimated BAG and examined its associations with cognitive performance, plasma biomarkers, and disruptions in key brain networks. This work seeks to clarify the clinical relevance of multimodal BAG and its potential as a marker of brain aging and network-level vulnerability in AD.

2. Methods

2.1. Study design and participants

This observational study was based on data from the Chinese Preclinical Alzheimer's Disease Study (CPAS) cohort[18]. The study was reviewed and approved by the Ethics Committee of Shanghai Sixth People's Hospital (approval number 2019–041). It was performed in accordance with the principles of the Declaration of Helsinki. All participants provided written informed consent to participate in the study. A total of 1094 participants were consecutively recruited from memory clinics and community settings between March 2019 and September 2024. Inclusion criteria included: native Chinese speakers aged ≥40 years; absence of severe visual or hearing impairments; and ability to complete the neuropsychological assessment protocol. Exclusion criteria included a history of alcohol or substance abuse; major psychiatric disorders, epilepsy, significant head trauma, stroke, or other severe neurological conditions; cognitive impairment attributable to non-Alzheimer's etiologies (e.g., Parkinson's disease, dementia with Lewy bodies, or frontotemporal dementia); and abnormal thyroid function or positive syphilis serology. Of the initially recruited participants, 48 were excluded due to non-AD-related cognitive disorders, 52 due to poor-quality imaging, four due to missing global cognitive assessments. After applying these criteria, 990 participants were included in the final analysis (see Fig. 1A for participant flow and data collection).

2.2. Neuropsychological assessment and diagnostic classification

All participants underwent a neuropsychological battery administered by trained neuropsychologists. General cognitive and functional assessments included the Montreal Cognitive Assessment–Basic (MoCA-B), Addenbrooke's Cognitive Examination III (ACE-III), Functional Activities Questionnaire (FAQ), and Activities of Daily Living (ADL). Memory was evaluated using the Auditory Verbal Learning Test (AVLT) and Brief Visuospatial Memory Test (BVMT); language by the Animal Fluency Test (AFT), Fruit Fluency Test (FFT), and Boston Naming Test (BNT); executive function by the Shape Trail Test A/B (STT-A/STT-B) and the Category Switching Test (CaST)[19]; and visuospatial ability by the Silhouettes Test (ST) and Judgment of Line Orientation (JLO).

Cognitive classification was based on established diagnostic criteria with defined operational thresholds.

Normal Cognition (NC) was defined by the absence of both subjective cognitive complaints and objective cognitive impairment, with preserved daily functioning.

Subjective Cognitive Decline (SCD) was defined according to the Subjective Cognitive Decline Initiative (SCD-I) framework[20], requiring the presence of self-reported cognitive complaints in the absence of objective cognitive impairment on neuropsychological testing and without functional impairment. Objective cognitive normality in both NC and SCD groups was determined using education-adjusted MoCA-B scores within the normal range, with intact ADL and FAQ performance.

Mild Cognitive Impairment (MCI) was diagnosed according to Petersen's criteria and operationalized as MoCA-B scores falling below education-adjusted cut-off values corresponding to approximately 1.5 standard deviations below normative means, in the absence of significant impairment in daily functioning[21,22].

Dementia was diagnosed based on the 2011 National Institute on Aging–Alzheimer's Association (NIA-AA) criteria for probable Alzheimer's disease, requiring both objective cognitive impairment and functional decline[23].

2.3. PET and MRI acquisition and processing

Cerebral Aβ deposition was assessed using [^{18}F]-florbetapir PET. Images were acquired on a Siemens Biograph mCT FlowMotion PET/CT scanner (Siemens Healthineers, Erlangen, Germany) at Huashan Hospital using a standardized protocol, and standardized uptake value ratios (SUVRs) were calculated using the whole cerebellum as the reference. Co-registration to T1-weighted MRI, partial volume correction, and region-wise SUVR extraction were performed using Statistical Parametric Mapping (SPM12; Wellcome Centre for Human Neuroimaging, UCL, London, UK) in MATLAB R2016b (MathWorks, Natick, MA, USA), based on the Automated Anatomical Labeling (AAL) atlas. Visual classification of Aβ positivity was independently rated by two nuclear medicine physicians.

High-resolution structural and resting-state functional MRI (rs-fMRI) scans were acquired on a 3T Siemens Prisma scanner (Siemens Healthineers, Erlangen, Germany) at Shanghai Sixth People's Hospital. Gray matter volume maps were derived from segmented T1 images and parcellated into AAL-defined regions for brain age modeling. rs-fMRI connectivity between the hippocampus and the default mode network (DMN) was calculated using a region-of-interest (ROI)-based approach

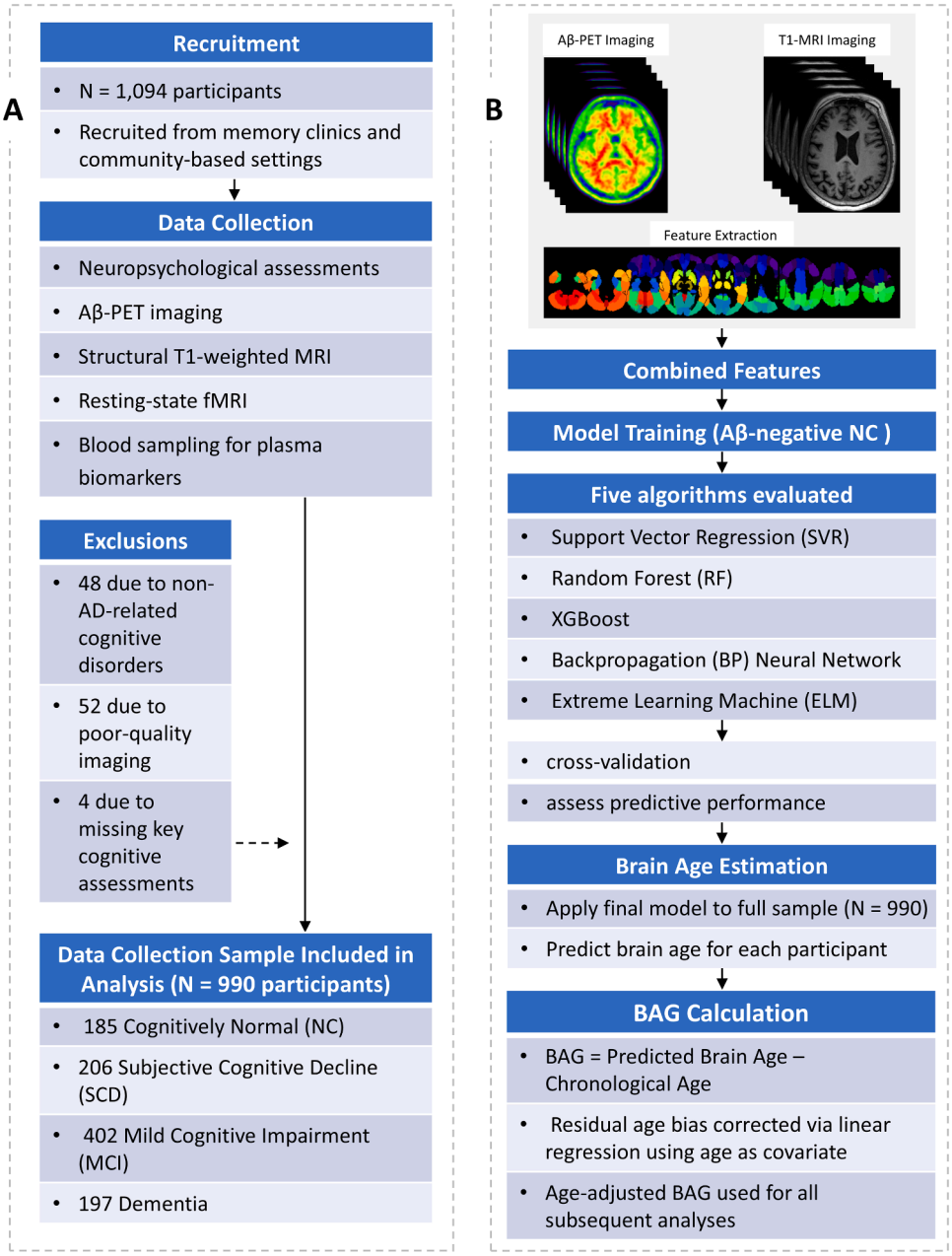

Fig. 1. Overview of participant recruitment and brain age modeling pipeline. Legend: Panel A, Flowchart of participant recruitment and data collection. A total of 1094 individuals were recruited from memory clinics and community-based settings, with 990 included in the final analysis after applying exclusion criteria. Included participants underwent comprehensive neuropsychological assessments, amyloid-PET imaging, structural MRI, resting-state fMRI, and blood sampling for plasma biomarkers. Panel B, Workflow for brain age prediction. Regional features extracted from Aβ-PET and T1-weighted MRI were combined and used to train brain age models using five machine learning algorithms, with training performed in Aβ-negative cognitively normal participants. After cross-validation, the optimal model was applied to the full sample to estimate brain age and compute brain age gap (BAG), defined as the difference between predicted and chronological age. Residual age bias was corrected using linear regression, and the adjusted BAG was used in all subsequent analyses.

[13]. Detailed acquisition parameters and preprocessing steps are provided in Supplementary Methods.

2.4. Plasma biomarkers

Peripheral blood samples were collected using standardized venipuncture procedures. Plasma levels of Aβ42, Aβ40, phosphorylated tau at threonine 181 (p-tau181), phosphorylated tau at threonine 217 (p-tau217), neurofilament light (NfL), and glial fibrillary acidic protein (GFAP) were measured using a fully automated immunoassay platform based on a light-initiated chemiluminescence method (Chemclin LiCA® 800 analyzer, Chemclin Diagnostics). This homogeneous sandwich immunoassay leverages laser-activated singlet oxygen transfer to trigger chemiluminescent reactions, enabling highly sensitive, wash-free detection with a broad linear range and strong anti-interference capabilities. Due to sample availability and batch processing constraints, complete data were available for up to 892 individuals for p-tau217 and GFAP, and for 809 individuals for Aβ42/40, p-tau181, and NfL. All assays were performed under blinded conditions following the manufacturer's protocols.

2.5. Brain age modeling and BAG calculation

Brain age modeling used region-wise Aβ-PET and T1-MRI features,

capturing complementary information on cortical pathology and gray matter morphology.

Brain age prediction models were developed within the MATLAB framework and included five commonly used algorithms: support vector regression (SVR), random forest (RF), extreme gradient boosting (XGBoost), backpropagation (BP) neural network, and extreme learning machine (ELM). Conceptual summaries of the five algorithms are included in the Supplementary Methods.

To identify the optimal algorithm, we performed nested 5-fold cross-validation on Aβ-negative participants within the NC group. The inner loop employed Bayesian optimization to search the hyperparameter space, whereas the outer loop trained and evaluated models using multimodal fusion features. The primary metric was mean absolute error (MAE), calculated separately for males and females; secondary metrics included root mean square error (RMSE), Pearson correlation coefficient, coefficient of determination (R^2), and systematic slope bias (ε-bias; $|\text{slope} - 1|$). R^2 quantifies the proportion of variance in chronological age explained by the predictions, while ε-bias assesses systematic deviation of predicted ages from chronological age. The difference between predicted and chronological age was defined as the BAG. After selecting the best-performing algorithm, we retained the Aβ-negative NC data partitioned by the 5-fold cross-validation splits and applied linear regression to the residuals (predicted age minus chronological age) to correct for age-related bias, yielding cross-fold bias-corrected MAE and BAG estimates.

Finally, the optimal algorithm was trained using Aβ-negative participants within the NC group, and the corresponding bias-correction procedure was derived and applied to subsequent analyses to ensure comparability and interpretability of BAG estimates. The final model was then applied to the remaining study sample, including amyloid-positive NC and participants with SCD, MCI, and dementia, to generate individualized brain-age estimates and bias-corrected BAG values. Single-modality analyses (PET-only or MRI-only) were conducted using the same algorithm and bias-correction framework.

2.6. Statistical analysis

All analyses were conducted in R (version 4.3.1). Group differences in demographic and clinical characteristics were examined using one-way analysis of variance (ANOVA) for continuous variables and chi-square tests for categorical variables, with a significance threshold of $p < 0.05$ (two-tailed).

To assess the association of BAG with cognitive status, multinomial logistic regression models were fitted with NC as the reference group and SCD, MCI, and dementia as outcomes. BAG was entered as the predictor of interest, with age, sex, and education as covariates. Odds ratios (ORs) with 95 % confidence intervals (CIs) and Wald p values were reported. To evaluate the discriminative performance of BAG for identifying cognitive impairment, receiver operating characteristic (ROC) analyses were conducted based on multivariable logistic regression models. To assess the incremental discriminative value of BAG, model performance before and after adding BAG was compared using changes in the area under the curve (AUC; ΔAUC), continuous Net Reclassification Index (NRI), and Integrated Discrimination Improvement (IDI), with uncertainty estimated using bootstrap resampling (1000 iterations).

The explanatory value of BAG for global cognition (ACE-III) was evaluated using general linear models (GLMs) and compared against models based on global amyloid burden (SUVR). Model performance was assessed with R^2 and Akaike Information Criterion (AIC). To further isolate the effect of BAG beyond SUVR and demographics, Residual-BAG was derived by regressing BAG on SUVR, age, sex, and education, and included in extended models.

Associations between BAG and plasma biomarkers were examined using partial correlations in both the overall cohort and cognitive subgroups. BAG–cognition associations were tested across domain-specific measures (executive, memory, language, visuospatial) using the same approach. BAG–functional connectivity associations were examined between hippocampal subregions and DMN targets in the overall cohort, controlling for the same covariates. Given the exploratory nature of these analyses, no correction for multiple comparisons was applied.

3. Results

3.1. Participant characteristics across cognitive status groups

A total of 990 participants were included in the analysis, comprising 185 NC, 206 with SCD, 402 with mild MCI, and 197 with dementia. Group-wise comparisons of demographic, clinical, and cognitive characteristics are summarized in Table 1. (Fig. 1A illustrates the participant flow and data collection process).

There were no significant differences in sex distribution across the groups ($\chi^2 = 0.34$, $p = 0.953$). Age increased significantly with disease severity, with participants in more advanced stages showing higher mean age ($F = 14.8$, $p < 0.001$). Years of education showed a decreasing trend across groups, with the dementia group having the lowest educational attainment ($F = 40.89$, $p < 0.001$). Aβ-PET positivity increased markedly from 18.9 % in the NC group to 77.7 % in the dementia group ($\chi^2 = 187.64$, $p < 0.001$), and global amyloid burden (SUVR) increased significantly with cognitive deterioration ($F = 90.57$, $p < 0.001$).

Functional capacity declined with increasing disease severity, as reflected by significant differences in ADL and FAQ scores (all $p < 0.001$). Global cognition, assessed using MoCA-B and ACE-III, exhibited differences across the cognitive spectrum, with progressively lower scores from NC to dementia (all $p < 0.001$). Across the cognitive continuum, participants showed progressive impairments in executive, memory, language, and visuospatial functions, with significant group differences observed across all domain-specific assessments (all $p < 0.001$). Executive function was assessed using STT-A/STT-B and the CaST; memory via AVLT and BVMT; language through AFT, FFT, and BNT; and visuospatial ability using ST and JLO.

3.2. Brain age and BAG

Brain age prediction was performed using five machine learning models: SVR, RF, XGBoost, BP, and ELM. Each model was trained on three sets of features: Aβ-PET features alone, T1-weighted MRI features alone, and a combined set of PET and MRI features. As detailed in Table S1, the SVR model consistently outperformed the others across all feature types. When using the combined feature set, SVR achieved the lowest MAE, with values of 5.44 years for males and 5.78 years for females. This represented an improvement over using PET or T1 features alone (MAE = 5.89/6.01 and 5.74/6.74 for males/females, respectively).

To further evaluate model robustness, we examined the performance of the cross-validated, bias-corrected SVR model. After bias correction, the average MAE was reduced to 3.48 years in males and 3.38 years in females, indicating stable performance under cross-validation.

Ultimately, after algorithm selection and robustness evaluation, we retrained the SVR model on the full Aβ-negative cognitively normal reference sample and derived a single bias-correction equation. This finalized, bias-corrected model was then fixed and used for all subsequent analyses across cognitive groups. This final model achieved MAE values of 2.07 years in males and 2.51 years in females, together with low systematic bias (ε-bias < 0.05) and satisfactory goodness-of-fit metrics ($R^2 = 0.88$ in males and 0.86 in females), supporting its suitability for generating brain-age estimates across cognitive groups.

In comparison, the RF model showed the second-best performance, with MAEs of 5.24 (male) and 6.03 (female) for the combined features, but it was still inferior to SVR. XGBoost and ELM yielded moderately higher MAEs, while the BP model performed the worst, with prediction

Table 1
Demographic, Clinical, and Cognitive Characteristics Across Cognitive Status Groups.

Variable	NC ($n = 185$)	SCD ($n = 206$)	MCI ($n = 402$)	Dementia ($n = 197$)	Stat	P value
Sex (male [%])	74 (40.0 %)	77 (37.4 %)	156 (38.8 %)	78 (39.6 %)	$\chi^2 = 0.34$	0.953
Age (year)	63.98 ± 8.46	63.26 ± 7.74	66.57 ± 7.08	67.47 ± 8.47	$F = 14.8$	<0.001
Education (year)	12.74 ± 3.35	12.55 ± 3.12	11.31 ± 3.39	9.28 ± 4.13	$F = 40.89$	<0.001
Aβ-PET (positive [%])	35 (18.9 %)	45 (21.8 %)	135 (33.6 %)	153 (77.7 %)	$\chi^2 = 187.64$	<0.001
Global SUVR	1.08 ± 0.08	1.09 ± 0.08	1.12 ± 0.12	1.28 ± 0.24	$F = 90.57$	<0.001
Brain Age (year)	63.98 ± 9.27	64.05 ± 8.21	68.00 ± 9.22	77.34 ± 10.66	$F = 89.09$	<0.001
BAG (year)	0.00 ± 3.80	0.79 ± 4.13	1.43 ± 5.34	9.87 ± 8.06	$F = 139.46$	<0.001
ADL	20.16 ± 0.78	20.32 ± 1.73	20.68 ± 3.56	24.29 ± 7.06	$F = 47.83$	<0.001
FAQ	0.26 ± 0.84	1.04 ± 3.38	1.17 ± 2.97	6.84 ± 6.81	$F = 117.93$	<0.001
MoCA-B	26.29 ± 2.11	25.57 ± 2.83	22.10 ± 3.76	12.74 ± 4.30	$F = 617.13$	<0.001
ACE-III	83.41 ± 7.40	81.59 ± 7.57	72.69 ± 9.24	48.62 ± 13.28	$F = 528.24$	<0.001
STT-A	47.38 ± 17.39	47.13 ± 14.84	55.77 ± 21.83	83.93 ± 39.51	$F = 63.64$	<0.001
STT-B	122.71 ± 36.17	123.26 ± 34.93	156.44 ± 55.39	208.34 ± 59.68	$F = 77.51$	<0.001
CaST	16.58 ± 4.84	15.45 ± 4.55	12.75 ± 4.44	9.30 ± 4.81	$F = 56.32$	<0.001
AVLT Short delay recall	6.26 ± 2.00	6.00 ± 2.06	3.14 ± 2.06	0.80 ± 1.28	$F = 236.83$	<0.001
AVLT Long delay recall	6.09 ± 2.00	5.66 ± 2.25	2.41 ± 1.94	0.51 ± 0.91	$F = 293.1$	<0.001
AVLT Recognition	22.10 ± 1.49	21.93 ± 1.64	19.02 ± 3.05	15.54 ± 4.59	$F = 163.89$	<0.001
BVMT Short delay recall	9.41 ± 2.70	9.09 ± 2.89	6.97 ± 3.39	1.72 ± 2.31	$F = 136.46$	<0.001
BVMT Long delay recall	9.47 ± 2.71	9.17 ± 2.94	6.88 ± 3.57	1.65 ± 2.44	$F = 127.07$	<0.001
BVMT Recognition	11.81 ± 0.56	11.60 ± 1.02	10.90 ± 1.81	8.04 ± 2.68	$F = 115.82$	<0.001
AFT	18.25 ± 4.18	17.78 ± 4.54	13.96 ± 4.14	10.01 ± 4.57	$F = 154.41$	<0.001
FFT	13.53 ± 3.15	13.53 ± 2.97	11.07 ± 2.92	6.94 ± 2.86	$F = 213.59$	<0.001
BNT	24.86 ± 2.63	24.66 ± 2.85	22.03 ± 4.05	18.92 ± 4.69	$F = 76.51$	<0.001
ST	10.16 ± 2.58	9.91 ± 2.71	8.75 ± 2.75	6.74 ± 3.05	$F = 36.85$	<0.001
JLO	21.78 ± 4.56	21.32 ± 3.69	19.72 ± 4.72	17.14 ± 5.48	$F = 23.74$	<0.001

Note: Global SUVR = global standardized uptake value ratio derived from amyloid PET; BAG = brain age gap; ADL = Activities of Daily Living; FAQ = Functional Activities Questionnaire; MoCA-*B* = Montreal Cognitive Assessment–Basic version; ACE-III = Addenbrooke's Cognitive Examination III; STT-A / STT-*B* = Shape Trail Test part A / part B; CaST = Category Switching Test; AVLT = Auditory Verbal Learning Test; BVMT = Brief Visuospatial Memory Test; AFT = Animal Fluency Test; FFT = Fruit Fluency Test; BNT = Boston Naming Test; ST = Silhouettes Test; JLO = Judgement of Line Orientation.

errors exceeding 11 years across all settings. Based on these results, the SVR model with fused PET and MRI features was selected as the final model for estimating brain age in subsequent analyses (see Fig. 1B).

Based on the SVR model with combined features, brain age estimates increased progressively with cognitive severity. As shown in Table 1, the mean predicted brain age rose from 63.98 ± 9.27 years in the NC group to 64.05 ± 8.21 in SCD, 68.00 ± 9.22 in MCI, and 77.34 ± 10.66 in dementia ($F = 89.09$, $p < 0.001$). Correspondingly, the BAG showed a progressive increase across groups, with values of −0.00 ± 3.80, 0.79 ± 4.13, 1.43 ± 5.34, and 9.87 ± 8.06 years, respectively ($F = 139.46$, $p < 0.001$). After stratification by amyloid PET status, BAG showed a progressive increase across cognitive stages in both Aβ-positive and Aβ-negative participants (Table S2, Supplementary Figure 1).

Based on the SVR model with combined features, estimated brain age increased progressively with cognitive severity. As shown in Table 1, the mean predicted brain age rose from 63.98 ± 9.27 years in the NC group to 64.05 ± 8.21 years in SCD, 68.00 ± 9.22 years in MCI, and 77.34 ± 10.66 years in dementia ($F = 89.09$, $p < 0.001$). Correspondingly, BAG increased across groups, with mean values of 0.00 ± 3.80, 0.79 ± 4.13, 1.43 ± 5.34, and 9.87 ± 8.06 years, respectively ($F = 139.46$, $p < 0.001$). After stratification by amyloid PET status, BAG continued to increase across cognitive stages in both Aβ-positive and Aβ-negative participants

3.3. Correlations between brain age, BAG, and chronological age

Fig. 2A displays the associations between predicted Brain Age and chronological age, as well as BAG and chronological age. In the overall sample, Brain Age showed a strong positive correlation with chronological age ($r = 0.78$, $p < 0.001$), indicating that the prediction model—which integrates regional Aβ-PET and MRI features—effectively captured normative age-related brain changes. In contrast, BAG was not significantly correlated with age ($r = 0.04$, $p = 0.25$), suggesting that BAG captures age-independent deviations in brain aging.

Across cognitive subgroups, the correlation between Brain Age and chronological age remained significant, though the strength declined with increasing cognitive impairment (NC: $r = 0.91$; SCD: $r = 0.87$; MCI: $r = 0.82$; Dementia: $r = 0.67$; all $p < 0.001$). This pattern indicates reduced model alignment with chronological age in later disease stages, possibly reflecting increasing heterogeneity in brain pathology.

For BAG, correlations with age were generally weak and inconsistent. In the NC group, BAG was uncorrelated with age ($r = 0$, $p = 1$), affirming its age-independent nature. However, weak but statistically significant negative correlations were observed in the SCD ($r = -0.15$, $p = 0.032$) and dementia groups ($r = -0.17$, $p = 0.017$), suggesting that in these stages, older individuals tended to exhibit slightly lower BAG values. No significant correlation was observed in the MCI group ($r = 0.08$, $p = 0.093$).

3.4. Relationship between BAG and cognitive status and discriminative performance

In models adjusted for age, sex, and education, each 1-year higher BAG was associated with higher odds of MCI (odds ratio [OR] = 1.08, 95 % confidence interval [CI] 1.04–1.12, $p < 0.001$) and dementia (OR = 1.37, 95 % CI 1.30–1.44, $p < 0.001$) in the overall cohort, with a trend for SCD (OR = 1.04, 95 % CI 1.00–1.08, $p = 0.086$). Associations were stronger among Aβ-positive individuals—SCD (OR = 1.13, 95 % CI 1.03–1.24, $p = 0.009$), MCI (OR = 1.16, 95 % CI 1.07–1.26, $p < 0.001$), and dementia (OR = 1.46, 95 % CI 1.33–1.60, $p < 0.001$)—whereas in the Aβ-negative stratum only dementia remained significant (OR = 1.21, 95 % CI 1.12–1.31, $p < 0.001$). See Table S3.

To further evaluate the relevance of BAG for risk stratification, we performed discrimination analyses focusing on objective cognitive impairment. Participants were categorized as objectively impaired (MCI and dementia) or objectively non-impaired (NC and SCD).

A base multivariable logistic regression model including age, sex, years of education, and APOE ε4 carrier status was specified. After adding BAG to this base model, discriminative performance reached an area under the curve (AUC) of 0.748 (95 % CI 0.717–0.779) in the overall cohort, 0.820 (95 % CI 0.776–0.864) among Aβ-positive participants, and 0.689 (95 % CI 0.646–0.731) in Aβ-negative participants

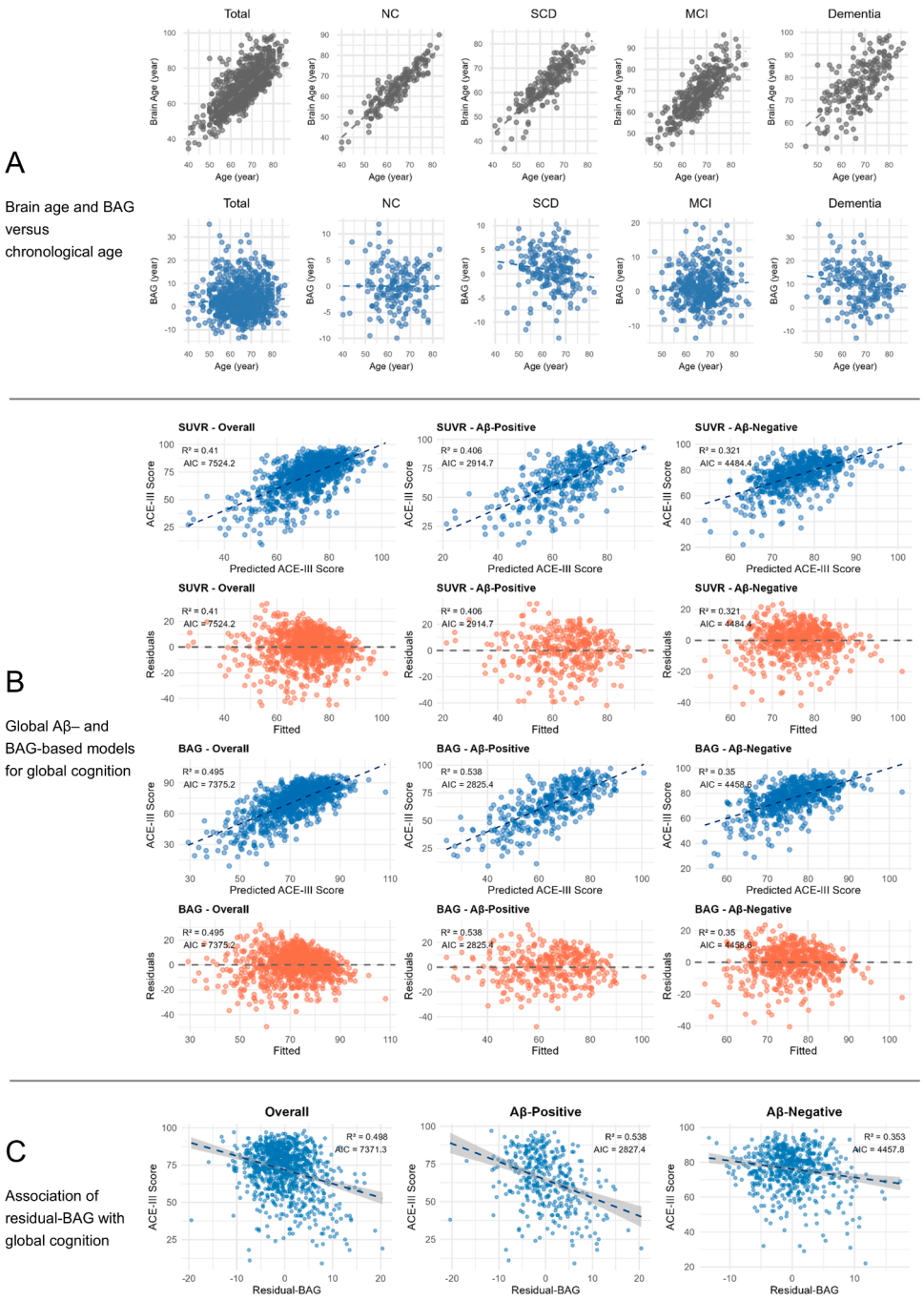

Fig. 2. Brain age estimation, group-wise associations, and cognitive relevance of the amyloid-informed brain age model. Legend: Panel A shows the relationship between predicted Brain Age and chronological age for the overall sample and for each cognitive subgroup (NC, SCD, MCI, Dementia), illustrating the accuracy of brain age estimation across the cognitive continuum. The lower plots depict the corresponding brain age gap (BAG) versus chronological age, revealing group-wise deviations in age-related BAG trajectories. Panel B presents model performance for explaining global cognitive function (ACE-III) using either global Aβ SUVR or BAG across the overall cohort, Aβ-positive, and Aβ-negative groups. Scatterplots and residual plots indicate that BAG consistently outperformed SUVR, as reflected by higher R^2 and lower AIC values. Panel C shows the relationship between Residual-BAG (the variance in BAG not explained by global Aβ) and ACE-III scores in the same three groups. Even after accounting for global Aβ, residual-BAG remained significantly associated with cognition, demonstrating that BAG provides additional explanatory information beyond amyloid burden as an integrative biomarker of amyloid-linked brain aging.

(Table S4 and Supplementary Figure 2).

Incremental discriminative value was quantified by comparing model performance before and after inclusion of BAG, showing increases in AUC (ΔAUC = 0.038, 95 % CI 0.019–0.058 in the overall cohort; ΔAUC = 0.098, 95 % CI 0.051–0.146 in Aβ-positive participants), with consistent improvements in continuous NRI and IDI (Table S5).

3.5. *Explanatory value of BAG for cognitive performance*

Fig. 2B–C illustrates the comparative performance of Global SUVR and BAG in explaining variance in global cognitive function, as measured by ACE-III, across the overall sample, Aβ-positive, and Aβ-negative groups.

In the base models (Fig. 2B), BAG consistently outperformed SUVR in explaining variance in ACE-III scores. In the overall sample, the BAG

model yielded a higher explained variance ($R^2 = 0.495$ vs. 0.410) and a lower (AIC (7375.2 vs. 7524.2) compared to the SUVR-based model. Similar patterns were observed in the Aβ-positive group, where BAG explained more variance in cognitive function ($R^2 = 0.538$ vs. 0.406) and showed a reduced AIC (2825.4 vs. 2914.7). Although model performance was overall lower in the Aβ-negative group, BAG still slightly outperformed SUVR ($R^2 = 0.350$ vs. 0.321; AIC = 4458.6 vs. 4484.4).

To address potential confounding by APOE genotype, sensitivity analyses additionally adjusted for APOE ε4 carrier status. After APOE adjustment, overall model fit improved across models, as reflected by lower AIC values. In the overall sample, after adjustment for APOE ε4 carrier status, the BAG model accounted for a greater proportion of variance in ACE-III scores than the global Aβ-SUVR model ($R^2 = 0.496$ vs. 0.409; AIC = 7077.3 vs. 7222.7), with consistent patterns observed in both Aβ-stratified subgroups (Supplementary Figure 3). These findings indicate that the superior cognitive association of BAG relative to global Aβ-SUVR is robust to APOE adjustment.

To assess the added explanatory value of BAG after accounting for global amyloid burden and demographics, Residual-BAG—calculated by regressing BAG on global SUVR, age, sex, and education—was included in an extended model (Fig. 2C). Incorporating Residual-BAG significantly improved model fit in the overall and Aβ-positive groups. In the overall sample, R^2 increased from 0.410 to 0.498 and AIC decreased from 7524.2 to 7371.3. Similarly, in the Aβ-positive group, R^2 rose from 0.406 to 0.538, accompanied by a reduction in AIC from 2914.7 to 2827.4. In the Aβ-negative group, Residual-BAG also yielded a modest

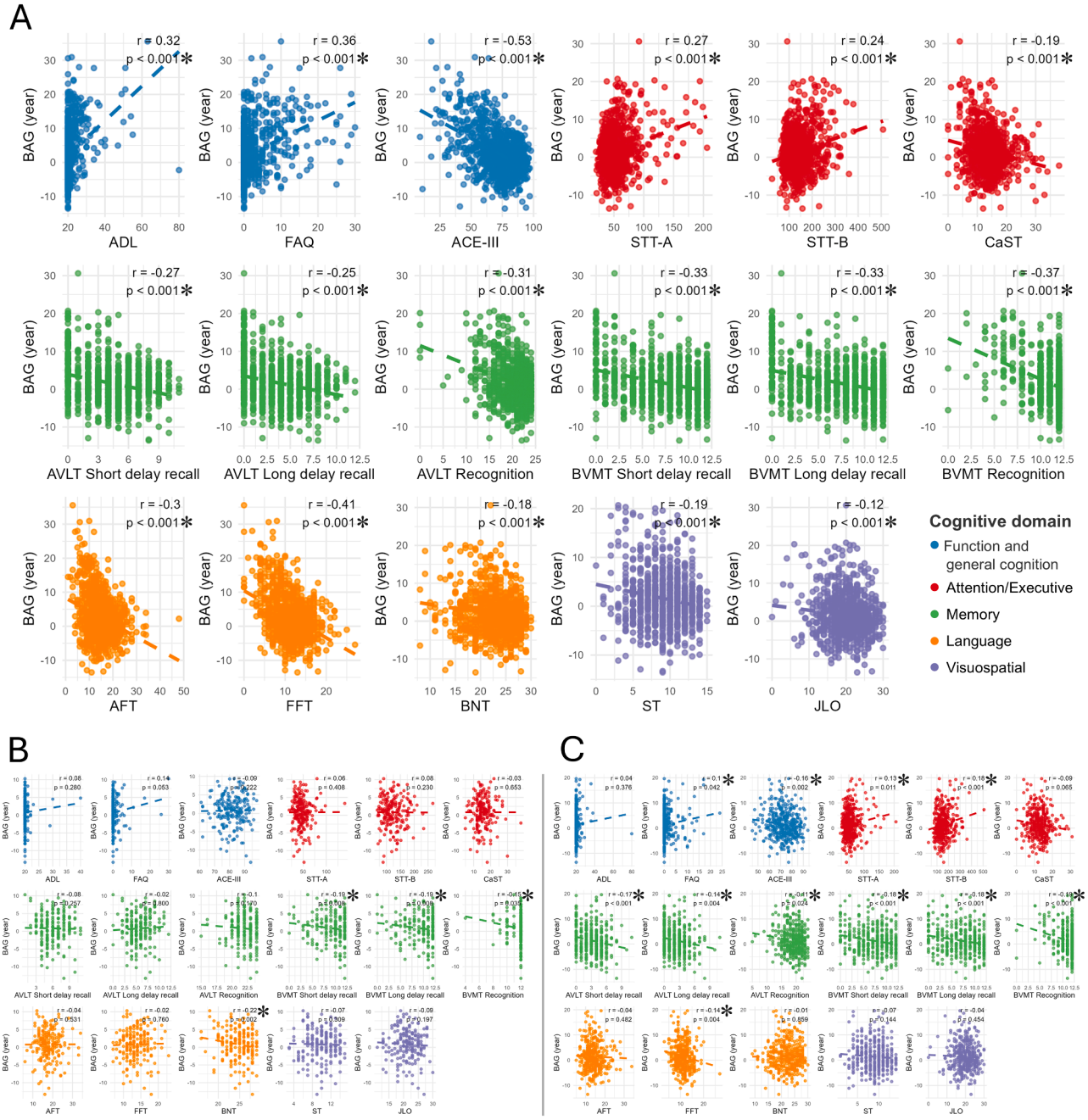

Fig. 3. Partial correlations between BAG and cognitive variables in the total sample and subgroups. Legend: Scatterplots show the associations between BAG and a range of cognitive measures across the total sample (panel A), the Subjective Cognitive Decline (SCD) group (panel B), and the Mild Cognitive Impairment (MCI) group (panel C). All analyses controlled for age, sex, and education. Asterisks (*) represent statistical significance.

improvement ($R^2 = 0.353$ vs. 0.321; AIC = 4457.8 vs. 4484.4), though the effect size was smaller.

These results demonstrate that BAG not only surpasses global SUVR in explaining global cognitive performance, particularly among individuals with elevated amyloid burden, but also captures additional information beyond global amyloid measures.

3.6. Associations between BAG and plasma biomarkers

Supplementary Figure 4 shows the partial correlations between BAG and plasma biomarkers—Aβ42/Aβ40, p-tau217, p-tau181, NfL, and GFAP—across the total sample and cognitive subgroups. All analyses were adjusted for age, sex, and education. In the total sample, BAG was significantly associated with all five biomarkers. Specifically, BAG correlated negatively with the Aβ42/Aβ40 ratio ($r = –0.10$, $p = 0.006$), and positively with p-tau217 ($r = 0.56$, $p < 0.001$), p-tau181 ($r = 0.35$, $p < 0.001$), NfL ($r = 0.24$, $p < 0.001$), and GFAP ($r = 0.43$, $p < 0.001$).

In subgroup analyses, the pattern of associations varied by cognitive status. In the NC group, none of the biomarkers showed significant associations with BAG. In the SCD group, only GFAP was significantly associated with BAG ($r = 0.16$, $p = 0.036$), suggesting early glial activation may reflect subtle aging-related brain changes in this stage. In the MCI group, BAG was positively correlated with p-tau217 ($r = 0.27$, $p < 0.001$), NfL ($r = 0.19$, $p < 0.001$), and GFAP ($r = 0.25$, $p < 0.001$), highlighting a convergence of tau, axonal, and glial pathologies with brain aging. The association with p-tau181 showed a trend toward significance ($r = 0.10$, $p = 0.071$), while Aβ42/Aβ40 was not significant. In the dementia group, BAG was significantly associated with Aβ42/Aβ40 ($r = –0.26$, $p < 0.001$), p-tau217 ($r = 0.49$, $p < 0.001$), p-tau181 ($r = 0.38$, $p < 0.001$), and GFAP ($r = 0.25$, $p < 0.001$). No association was observed with NfL ($p = 0.814$).

Group-level distributions of plasma biomarkers across the four cognitive groups are provided in Table S6.

3.7. Associations between BAG and cognitive performance

In the total sample, BAG was significantly associated with a broad range of cognitive measures, as shown in Fig. 3A. Higher BAG values were correlated with poorer global cognitive function (ACE-III: $r = –0.53$, $p < 0.001$), increased functional impairment (ADL: $r = 0.32$; FAQ: $r = 0.36$; both $p < 0.001$), and reduced executive functioning (STT-A: $r = 0.27$; STT-B: $r = 0.24$; CaST: $r = –0.19$; all $p < 0.001$). Significant negative correlations were also observed between BAG and memory performance, including AVLT short delay recall ($r = –0.27$), long delay recall ($r = –0.25$), and recognition ($r = –0.31$), as well as BVMT short delay ($r = –0.33$), long delay ($r = –0.33$), and recognition scores ($r = –0.37$) (all $p < 0.001$). In the language domain, BAG was negatively associated with performance on the AFT ($r = –0.30$), FFT ($r = –0.41$), and BNT ($r = –0.18$). Visuospatial function also declined with increasing BAG, as reflected by negative correlations with the ST ($r = –0.19$) and the JLO ($r = –0.12$) (all $p < 0.001$).

In the SCD group, BAG was significantly associated with performance in select memory and language domains (Fig. 3B). Specifically, higher BAG was related to poorer visuospatial memory, as reflected by negative correlations with BVMT short delay recall ($r = –0.19$, $p = 0.008$), long delay recall ($r = –0.19$, $p = 0.008$), and recognition scores ($r = –0.15$, $p = 0.035$). In addition, BAG was negatively associated with naming ability on the BNT ($r = –0.22$, $p = 0.002$).

In the MCI group (Fig. 3C), higher BAG correlated with poorer global cognitive performance (ACE-III: $r = –0.16$, $p = 0.002$) and greater functional difficulties (FAQ: $r = 0.10$, $p = 0.042$). Executive function showed significant associations, with positive correlations between BAG and both STT-A ($r = 0.13$, $p = 0.011$) and STT-B ($r = 0.18$, $p < 0.001$), suggesting slower processing speed in individuals with older-appearing brains. BAG also exhibited consistent negative correlations with memory performance. This included AVLT short delay recall ($r = –0.17$, $p < 0.001$), long delay recall ($r = –0.14$, $p = 0.004$), and recognition ($r = –0.11$, $p = 0.024$), as well as BVMT short delay ($r = –0.18$, $p < 0.001$), long delay ($r = –0.18$, $p < 0.001$), and recognition scores ($r = –0.19$, $p < 0.001$). Additionally, association was observed between BAG and verbal fluency (FFT: $r = –0.14$, $p = 0.004$).

To further account for genetic risk, sensitivity analyses were conducted using partial correlation models with additional adjustment for APOE ε4 carrier status. After APOE adjustment, the overall pattern of associations between BAG and cognitive performance remained largely consistent, with modest attenuation of effect sizes across most measures. Importantly, the direction of associations was preserved, and BAG continued to show significant associations with global cognition, functional measures, and multiple memory- and executive-related outcomes in the total sample. In subgroup analyses, associations in the SCD and MCI groups were partially attenuated after APOE adjustment, whereas key memory- and executive-related measures—particularly in the MCI group—remained significantly associated with BAG. The original and APOE-adjusted partial correlation results are provided in Tables S7 and S8, respectively.

3.8. Associations between BAG and hippocampus-to-DMN functional connectivity

Fig. 4 illustrates the partial correlations between BAG and resting-state functional connectivity from hippocampal subregions to DMN targets, analyzed separately for the left (L-HC) and right hippocampus (R-HC). All correlations were adjusted for age, sex, and education. DMN targets included the anterior medial prefrontal cortex (amPFC), ventromedial prefrontal cortex (vmPFC), dorsomedial prefrontal cortex (dmPFC), precuneus (PRC), left and right intraparietal cortex (LIPC, RIPC), lateral temporal cortex (LLTC, RLTC), and parahippocampal formation (LPHF, RPHF).

In the L-HC, BAG was significantly negatively correlated with connectivity to the amPFC ($r = –0.18$, $p < 0.001$), LIPC ($r = –0.12$, $p = 0.020$), RIPC ($r = –0.22$, $p < 0.001$), and dmPFC ($r = –0.18$, $p < 0.001$). These results suggest that greater brain age is associated with weakened integration between the L-HC and both medial prefrontal and parietal DMN components. In the R-HC, BAG was also negatively associated with connectivity to several DMN regions, including the amPFC ($r = –0.13$, $p = 0.011$), LIPC ($r = –0.11$, $p = 0.031$), vmPFC ($r = –0.13$, $p = 0.015$), dmPFC ($r = –0.12$, $p = 0.026$), and LLTC ($r = –0.11$, $p = 0.043$). No significant associations were observed for hippocampal connections to PRC, lateral temporal cortex (RLTC), or parahippocampal regions (LPHF, RPHF).

4. Discussion

This study aimed to evaluate the clinical significance of a regional amyloid-informed multimodal BAG, derived from a multimodal model combining Aβ-PET and structural MRI, across the cognitive continuum spanning normal aging to AD. Using a large and deeply phenotyped cohort, we demonstrated that BAG was significantly associated with cognitive performance, AD-related plasma biomarkers, and hippocampus–DMN functional connectivity. These findings suggest that multimodal BAG may serve as an integrative marker reflecting both structural and pathological brain aging, offering potential utility for early risk stratification and disease monitoring in AD.

Our results demonstrated a progressive increase in BAG across the cognitive continuum. This finding supports the notion that BAG reflects accelerated brain aging linked to disease progression. Notably, in the SCD group, BAG showed a modest negative correlation with chronological age, indicating that younger individuals with subjective complaints may harbor a heavier pathological burden—consistent with prior evidence identifying early-onset SCD as a potentially more aggressive phenotype[24,25]. A similar inverse association observed in the dementia group may reflect a stage-dependent brain aging trajectory in

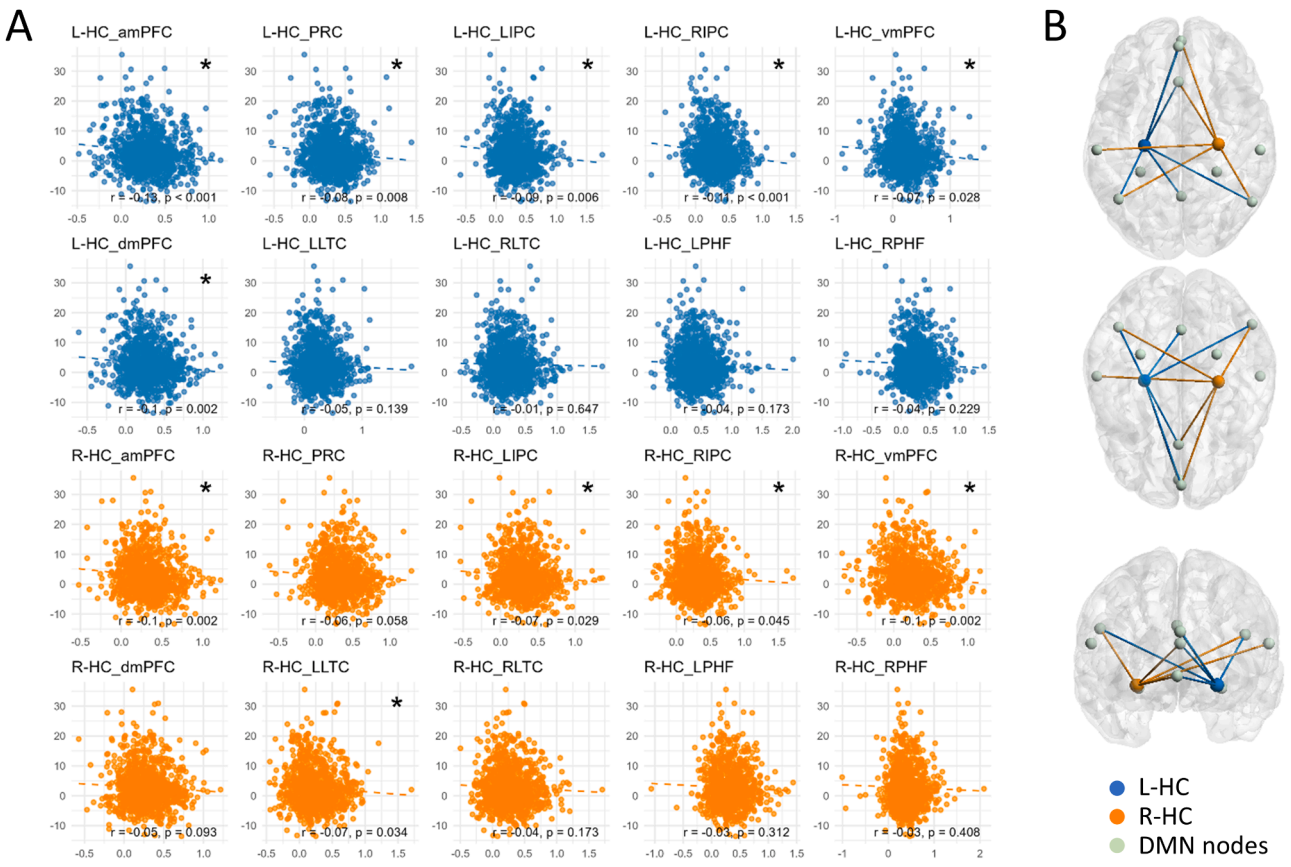

Fig. 4. Associations between BAG and hippocampus-to-DMN functional connectivity. Legend: Panel A: Partial correlation coefficients (r) between BAG and resting-state functional connectivity from hippocampal subregions to distributed default mode network (DMN) regions, adjusted for age, sex, and education. Each point represents a specific hippocampus–DMN connection. Blue points denote connections from the left hippocampus (L-HC), and orange points denote those from the right hippocampus (R-HC). Asterisks (*) indicate statistically significant associations ($p < 0.05$). Panel B: Hemispheric asymmetry of hippocampus–DMN connectivity associated with BAG. The plot visualizes differences in BAG-related connectivity between left and right hippocampal pathways, highlighting lateralization patterns. Region abbreviations: amPFC – anterior medial prefrontal cortex; PRC – precuneus; LIPC – left intraparietal cortex; RIPC – right intraparietal cortex; vmPFC – ventromedial prefrontal cortex; dmPFC – dorsomedial prefrontal cortex; LLTC – left lateral temporal cortex; RLTC – right lateral temporal cortex; LPHF – left parahippocampal formation; RPHF – right parahippocampal formation; L-HC – left hippocampus; R-HC – right hippocampus.

which pathology-related biological brain aging changes gradually reach a plateau[14,26], leading predicted brain age to stabilize, while chronological age continues to increase, thereby compressing the difference between biological and chronological age and resulting in a weak negative association between BAG and age.

Beyond these cross-sectional group differences, longer BAG was also associated with greater odds of cognitive impairment, with effects most pronounced in Aβ-positive individuals. Associations were significant for MCI and dementia, and even SCD showed a detectable signal—reaching significance in the Aβ-positive stratum and a borderline trend in the overall cohort. These findings highlight the sensitivity of amyloid-informed BAG to very early symptomatic changes and reinforce its value as an integrative marker of disease-relevant brain aging.

Moreover, when compared to Aβ-PET SUVR, BAG showed superior performance in explaining global cognition. Adjustment-based analyses further showed that residual BAG remained associated with cognitive status after accounting for global amyloid burden. In parallel, discrimination analyses demonstrated the incremental value of BAG beyond established demographic and genetic factors. Together, these findings support the added value of multimodal BAG as an integrative marker of brain vulnerability. This observation is consistent with prior studies indicating that multimodal brain-age models may better capture the biological heterogeneity of brain aging and show greater sensitivity to cognitive impairment than unimodal models[27,28].

BAG was significantly associated with both core and non-core blood-based biomarkers of AD pathology. Specifically, higher BAG correlated with elevated levels of plasma p-tau217, p-tau181, NfL, and GFAP, while showing a negative association with the Aβ42/Aβ40 ratio. These results indicate that BAG reflects a wide range of AD-related pathophysiological processes, including amyloid accumulation, tauopathy, axonal degeneration, and astroglial activation. Blood biomarkers have emerged as promising and scalable tools for early AD detection and staging, owing to their accessibility and sensitivity to neuropathological changes[9,29]. While prior studies have reported associations between unimodal brain age estimates and plasma p-tau levels[30,31], to our knowledge, no research has comprehensively evaluated how a multimodal BAG relates to an array of plasma biomarkers covering both core and ancillary AD-related mechanisms. Our findings thus provide novel evidence supporting the sensitivity of multimodal BAG to a broader spectrum of neurobiological alterations, reinforcing its role as an integrative imaging-derived marker bridging biological brain aging and peripheral biomarkers.

However, BAG did not show significant correlations with plasma biomarkers in the NC group. This may reflect the limited sensitivity of blood markers to detect early brain changes, whereas multimodal BAG could be more effective in capturing preclinical pathology and associated risk factors[32]. Our prior findings also suggested that regional Aβ-PET alterations may precede measurable changes in plasma biomarkers, lending further support to this interpretation[14].

In the SCD group, BAG was significantly associated only with GFAP, with no significant correlations observed for other plasma markers. As a marker of astroglial activation, GFAP has gained increasing attention for

its early responsiveness to amyloid pathology[33]. Notably, GFAP levels have been shown to rise during the SCD stage, prior to clinical deterioration, highlighting astrocytosis as one of the earliest biological responses in preclinical AD[34]. Recent studies further demonstrated that plasma GFAP is elevated in individuals with Aβ deposition even in the absence of objective cognitive deficits and is independently associated with amyloid PET, but not with tau PET[35]. These findings may explain why BAG is preferentially associated with GFAP in SCD, as it likely reflects subtle glial-driven changes that remain undetectable by other peripheral biomarkers. Overall, this reinforces the utility of BAG in detecting early neuroinflammatory signals and underscores the pivotal role of astroglial activation in the initial pathophysiological cascade of AD.

BAG also demonstrated significant associations with cognitive performance, reflecting its close relationship with overall cognitive functioning. These findings underscore the broad relevance of BAG to neurocognitive decline, suggesting that accelerated biological brain aging contributes meaningfully to cognitive deterioration across the Alzheimer's disease continuum.

In the SCD subgroup, associations between BAG and cognition were relatively limited, but notable in specific domains such as visual memory and naming ability. This pattern suggests that subtle neural alterations may already be detectable in individuals with subjective cognitive complaints, potentially signaling early pathological changes. At this stage, recognizing domain-specific vulnerabilities is crucial for the appropriate selection of cognitive assessments. Previous research has shown that visual and auditory memory exhibit distinct sensitivities to AD-related risk factors and pathology[36]. In preclinical individuals, visual memory decline may relate to subtle pathological changes and hippocampal subfield alterations[37]. Furthermore, naming ability has been shown to differ between cognitively normal individuals and preclinical AD groups, and has been associated with underlying AD pathology[38,39].

In the MCI stage, BAG showed stronger and broader associations with cognitive performance, particularly in global cognition, episodic memory, and executive function. Significant correlations with auditory memory and verbal fluency further indicate that BAG reflects widespread cognitive dysfunction as the disease progresses. These findings support BAG as a sensitive marker of cognitive decline in MCI, consistent with evidence that neuropsychological deficits predict dementia conversion[40], and that biological brain age better tracks cognitive and functional decline than chronological age[41]. Longitudinal studies have also shown steeper BAG increases in MCI individuals who convert to AD, highlighting its value as a dynamic marker of neurodegeneration [42].

BAG was significantly associated with reduced functional connectivity between the hippocampus and key regions of the DMN, particularly the medial prefrontal and parietal cortices. Specifically, higher BAG corresponded to decreased connectivity between the left hippocampus and medial prefrontal areas, as well as bilateral intraparietal cortices—connections involved in episodic retrieval, self-referential thought, and cognitive regulation[43]. In contrast, the right hippocampus exhibited disrupted connectivity with the medial prefrontal cortex, left parietal, and lateral temporal regions, which are more implicated in semantic processing and affective modulation. Emerging evidence emphasizes the central role of hippocampal–prefrontal circuits in supporting flexible cognition, such as hypothesis testing and compositional reasoning, through dynamic cross-talk between the hippocampus and medial prefrontal cortex[44,45]. Meanwhile, functional MRI (fMRI) studies suggest that medial temporal and parietal regions jointly contribute to autobiographical memory, integrating both episodic and semantic content[46]. Additionally, parietal–hippocampal repetitive transcranial magnetic stimulation (rTMS) has been shown to enhance DMN connectivity and improve cognition in AD, highlighting the role of the hippocampal–parietal–DMN axis in supporting cognitive function[47].

In addition, we observed asymmetric patterns in hippocampal–DMN connectivity, aligning with prior evidence of hemispheric differences in DMN organization and hippocampal integration. Greater left-lateralization, particularly in posterior DMN regions, has been linked to better verbal memory and preserved cognition in aging and early AD [48]. The left hippocampus also shows stronger causal interactions with DMN nodes than the right[49], and reduced DMN lateralization has been associated with cognitive decline in AD[50]. These findings highlight the significance of lateralization as a relevant dimension in understanding DMN vulnerability. Overall, BAG may reflect network-level decoupling related to brain aging, wherein disrupted hippocampal–DMN connections compromise neural integration supporting broad cognitive functions.

Taken together, the observed associations between BAG, domain-specific cognitive deficits, and hippocampus–DMN functional connectivity suggest a convergent network-level mechanism linking accelerated biological brain aging to cognitive vulnerability. BAG was most consistently related to global cognition, episodic memory, and executive function, with episodic memory being particularly dependent on hippocampal–DMN integrity[51,52]. Prior work has shown that alterations in DMN-related functional connectivity, particularly involving the hippocampus, are closely related to memory and higher-order cognitive performance and reflect early vulnerability to Alzheimer's disease–related pathology, even in preclinical risk states[51,53–55]. Disruption of medial temporal lobe–DMN interactions has been proposed as a systems-level mechanism underlying domain-specific cognitive impairment across aging and Alzheimer's disease phenotypes[52, 56]. This domain-specific convergence suggests the potential value of BAG as an integrative marker of accelerated biological brain aging that may confer network-level vulnerability and downstream domain-specific cognitive consequences.

While this study provides converging evidence for the clinical and biological relevance of amyloid-informed BAG, several limitations should be noted. First, its cross-sectional design precludes causal inference between BAG, cognitive decline, and biomarker changes; longitudinal follow-up is required to evaluate predictive value. Second, the multimodal model incorporated Aβ-PET and structural MRI but did not include other relevant pathologies such as tau or vascular burden. Third, the cohort includes participants recruited from both community settings and memory clinics, which may introduce selection bias and limit generalizability to the broader population. Finally, despite adjusting for demographics, unmeasured factors such as lifestyle or metabolic variables may still influence BAG.

5. Conclusion

In summary, this study demonstrates that amyloid-informed BAG serves as a sensitive marker linking accelerated brain aging with cognitive decline, plasma pathology, and hippocampal–DMN connectivity disruptions across the Alzheimer's continuum. Higher BAG was associated with an increased likelihood of cognitive impairment, most prominently in Aβ-positive individuals and detectable even at the SCD stage. Moreover, BAG correlated with both core and non-core plasma biomarkers and reflected multidomain cognitive deficits, capturing network-level aging processes that compromise neural integration. Together, these findings support multimodal BAG as a valid and scalable marker of biological brain aging, offering a unified framework that connects structural degeneration, AD pathology, and functional disconnection to explain individual variability in aging trajectories and disease progression.

Ethics approval and consent to participate

The study was reviewed and approved by the Ethics Committee of Shanghai Sixth People's Hospital (approval number 2019–041). It was performed in accordance with the principles of the Declaration of

Helsinki.

Consent for publication

Not applicable.

Declaration of generative AI and AI-assisted technologies in the writing process

During the preparation of this work the authors used ChatGPT in order to improve readability. After using this tool/service, the authors reviewed and edited the content as needed and take full responsibility for the content of the published article.

Data sharing statement

Deidentified participant data from this study (including clinical variables, imaging-derived BAG metrics, and statistical code) contain potentially sensitive participant information and are therefore not publicly available. Data and code will be made available upon reasonable request to the corresponding author, subject to institutional review and data use agreements. The study protocol and analysis scripts will be provided upon request for non-commercial academic research.

Funding

This work was supported by the National Natural Science Foundation of China (82171198, 62303295), the Shanghai Municipal Science and Technology Major Project (no. 2018SHZDZX01), the Scientific Research Project of Shanghai Municipal Health Commission (202340080) and Shanghai Municipal Health Commission (202140042, 202340173).

CRediT authorship contribution statement

Liang Cui: Writing – original draft. **Qing-Min Wang:** Writing – review & editing, Writing – original draft. **Zhen Zhang:** Methodology, Data curation. **Min Wang:** Methodology, Funding acquisition, Formal analysis. **You-Yi Tu:** Methodology, Data curation. **Jie-Hui Jiang:** Software, Conceptualization. **Yi-Hui Guan:** Resources. **Yue-Hua Li:** Software, Resources. **Fang Xie:** Validation, Resources. **Qi-Hao Guo:** Project administration, Funding acquisition, Conceptualization.

Declaration of competing interest

The authors declare that they have no known competing financial interests or personal relationships that could have appeared to influence the work reported in this paper.

Acknowledgments

We would like to thank Jie-Hua Zhu, Xiang-Qing Xie, and Yun Yang for their help with neuropsychological tests.

Supplementary materials

Supplementary material associated with this article can be found, in the online version, at doi:10.1016/j.tjpad.2026.100501.

References

[1] Gustavsson A, Norton N, Fast T, Frölich L, Georges J, Holzapfel D, et al. Global estimates on the number of persons across the Alzheimer's disease continuum. Alzheimer's Dement 2022;19:658–70. https://doi.org/10.1002/alz.12694.
[2] Mecocci P, Boccardi V. The impact of aging in dementia: it is time to refocus attention on the main risk factor of dementia. Ageing Res Rev 2021;65:101210. https://doi.org/10.1016/j.arr.2020.101210.
[3] Marseglia A, Dartora C, Samuelsson J, Poulakis K, Mohanty R, Shams S, et al. Biological brain age and resilience in cognitively unimpaired 70-year-old individuals. Alzheimer's Dement 2025;21:e14435. https://doi.org/10.1002/alz.14435.
[4] J S, L W, Y G, Y H, S C, S W, et al. Discovery of high-risk clinical factors that accelerate brain aging in adults: a population-based machine learning study. Research (Washington, DC) 2024;7. https://doi.org/10.34133/research.0500.
[5] Baecker L, Garcia-Dias R, Vieira S, Scarpazza C, Mechelli A. Machine learning for brain age prediction: introduction to methods and clinical applications. EBioMedicine 2021;72:103600. https://doi.org/10.1016/j.ebiom.2021.103600.
[6] Millar PR, Gordon BA, Luckett PH, Benzinger TL, Cruchaga C, Fagan AM, et al. Multimodal brain age estimates relate to Alzheimer disease biomarkers and cognition in early stages: a cross-sectional observational study. Elife 2023;12:e81869. https://doi.org/10.7554/eLife.81869.
[7] Lee J, Burkett BJ, Min H-K, Senjem ML, Lundt ES, Botha H, et al. Deep learning-based brain age prediction in normal aging and dementia. Nat Aging 2022;2:412–24. https://doi.org/10.1038/s43587-022-00219-7.
[8] Moguilner S, Baez S, Hernandez H, Migeot J, Legaz A, Gonzalez-Gomez R, et al. Brain clocks capture diversity and disparities in aging and dementia across geographically diverse populations. Nat Med 2024;30:3646–57. https://doi.org/10.1038/s41591-024-03209-x.
[9] Jack CR, Andrews JS, Beach TG, Buracchio T, Dunn B, Graf A, et al. Revised criteria for diagnosis and staging of Alzheimer's disease: Alzheimer's Association Workgroup. Alzheimers Dement 2024. https://doi.org/10.1002/alz.13859.
[10] Ozlen H, Pichet Binette A, Köbe T, Meyer P-F, Gonneaud J, St-Onge F, et al. Spatial extent of amyloid-β levels and associations with tau-PET and cognition. JAMA Neurol 2022;79:1025–35. https://doi.org/10.1001/jamaneurol.2022.2442.
[11] Grothe MJ, Barthel H, Sepulcre J, Dyrba M, Sabri O, Teipel SJ, et al. In vivo staging of regional amyloid deposition. Neurology 2017;89:2031–8. https://doi.org/10.1212/WNL.0000000000004643.
[12] Mattsson N, Palmqvist S, Stomrud E, Vogel J, Hansson O. Staging β-amyloid pathology with amyloid positron emission tomography. JAMA Neurol 2019;76:1319–29. https://doi.org/10.1001/jamaneurol.2019.2214.
[13] Cui L, Zhang Z, Tu Y, Wang M, Guan Y, Li Y, et al. Association of precuneus Aβ burden with default mode network function. Alzheimer's Dement 2025;21:e14380. https://doi.org/10.1002/alz.14380.
[14] Cui L, Zhang Z, Huang C-C, Yuan C-Y, Tu Y-Y, Wang M, et al. Beyond binary classification: comparing three region-based multi-phase aβ staging systems. Alzheimer's Dement 2025;21:e70253. https://doi.org/10.1002/alz.70253.
[15] Rodrigue KM, Kennedy KM, Devous S MD, Rieck JR, Hebrank AC, Diaz-Arrastia R, et al. β-amyloid burden in healthy aging: regional distribution and cognitive consequences. Neurology 2012;78:387. https://doi.org/10.1212/WNL.0b013e318245d295.
[16] Villemagne VL, Burnham S, Bourgeat P, Brown B, Ellis KA, Salvado O, et al. Amyloid β deposition, neurodegeneration, and cognitive decline in sporadic Alzheimer's disease: a prospective cohort study. Lancet Neurol 2013;12:357–67. https://doi.org/10.1016/S1474-4422(13)70044-9.
[17] Sengupta U, Kayed R. Amyloid β, Tau, and α-synuclein aggregates in the pathogenesis, prognosis, and therapeutics for neurodegenerative diseases. Prog. Neurobiol. 2022;214:102270. https://doi.org/10.1016/j.pneurobio.2022.102270.
[18] Cui L, Huang L, Pan F-F, Wang Y, Huang Q, Guan Y-H, et al. Chinese preclinical Alzheimer's Disease Study (C-PAS): design and challenge from PET acceptance. J Prevent Alzheimer's Dis 2023;10:571–80. https://doi.org/10.14283/jpad.2023.49.
[19] Cui L, Zhang Z, Guo Y, Li Y, Xie F, Guo Q. Category switching test: a brief amyloid-β-sensitive assessment tool for mild cognitive impairment. Assessment 2024;31:543–56. https://doi.org/10.1177/10731911231167537.
[20] Jessen F, Amariglio RE, Buckley RF, van der Flier WM, Han Y, Molinuevo JL, et al. The characterisation of subjective cognitive decline. Lancet Neurol 2020;19:271–8. https://doi.org/10.1016/S1474-4422(19)30368-0.
[21] Huang L, Chen K, Lin B, Tang L, Zhao Q, Lv Y, et al. Chinese version of Montreal Cognitive Assessment Basic for discrimination among different severities of Alzheimer's disease. Neuropsychiatr Dis Treatm 2018;14:2133–40. https://doi.org/10.2147/NDT.S174293.
[22] Petersen RC. Mild cognitive impairment as a diagnostic entity. J Intern Med 2004;256:183–94. https://doi.org/10.1111/j.1365-2796.2004.01388.x.
[23] McKhann GM, Knopman DS, Chertkow H, Hyman BT, Jack CR, Kawas CH, et al. The diagnosis of dementia due to Alzheimer's disease: recommendations from the National Institute on Aging-Alzheimer's Association workgroups on diagnostic guidelines for Alzheimer's disease. Alzheimers Dement 2011;7:263–9. https://doi.org/10.1016/j.jalz.2011.03.005.
[24] Pike KE, Cavuoto MG, Li L, Wright BJ, Kinsella GJ. Subjective cognitive decline: level of risk for future dementia and mild cognitive impairment, a meta-analysis of longitudinal studies. Neuropsychol Rev 2022;32:703–35. https://doi.org/10.1007/s11065-021-09522-3.
[25] Cedres N, Machado A, Molina Y, Diaz-Galvan P, Hernández-Cabrera JA, Barroso J, et al. Subjective cognitive decline below and above the age of 60: a multivariate study on neuroimaging, cognitive, clinical, and demographic measures. J Alzheimers Dis 2019;68:295–309. https://doi.org/10.3233/JAD-180720.
[26] O'Dell RS, Mecca AP, Chen M-K, Naganawa M, Toyonaga T, Lu Y, et al. Association of Aβ deposition and regional synaptic density in early Alzheimer's disease: a PET imaging study with [11C]UCB-J. Alzheimers Res Ther 2021;13:11. https://doi.org/10.1186/s13195-020-00742-y.
[27] Liem F, Varoquaux G, Kynast J, Beyer F, Kharabian Masouleh S, Huntenburg JM, et al. Predicting brain-age from multimodal imaging data captures cognitive

impairment. Neuroimage 2017;148:179–88. https://doi.org/10.1016/j.neuroimage.2016.11.005.
[28] Dörfel RP, Arenas-Gomez JM, Svarer C, Ganz M, Knudsen GM, Svensson JE, et al. Multimodal brain age prediction using machine learning: combining structural MRI and 5-HT2AR PET-derived features. Geroscience 2024;46:4123–33. https://doi.org/10.1007/s11357-024-01148-6.
[29] Blennow K, Galasko D, Perneczky R, Quevenco F-C, van der Flier WM, Akinwonmi A, et al. The potential clinical value of plasma biomarkers in Alzheimer's disease. Alzheimers Dement 2023;19:5805–16. https://doi.org/10.1002/alz.13455.
[30] Abughofah Y, Deardorff R, Vosmeier A, Hottle S, Dage JL, Dempsey D, et al. Association between BrainAGE and Alzheimer's disease biomarkers. Alzheimers Dement (Amst) 2025;17:e70094. https://doi.org/10.1002/dad2.70094.
[31] Kuchcinski G, Rumetshofer T, Zervides KA, Lopes R, Gautherot M, Pruvo J-P, et al. MRI BrainAGE demonstrates increased brain aging in systemic lupus erythematosus patients. Front Aging Neurosci 2023;15:1274061. https://doi.org/10.3389/fnagi.2023.1274061.
[32] Cumplido-Mayoral I, Brugulat-Serrat A, Sánchez-Benavides G, González-Escalante A, Anastasi F, Milà-Alomà M, et al. The mediating role of neuroimaging-derived biological brain age in the association between risk factors for dementia and cognitive decline in middle-aged and older individuals without cognitive impairment: a cohort study. Lancet Healthy Longev 2024;5:e276–86. https://doi.org/10.1016/S2666-7568(24)00025-4.
[33] Kim KY, Shin KY, Chang K-A. GFAP as a potential biomarker for Alzheimer's disease: a systematic review and meta-analysis. Cells 2023;12:1309. https://doi.org/10.3390/cells12091309.
[34] Liu Z, Shi D, Cai Y, Li A, Lan G, Sun P, et al. Pathophysiology characterization of Alzheimer's disease in South China's aging population: for the Greater-Bay-Area Healthy Aging Brain Study (GHABS). Alzheimers Res Ther 2024;16:84. https://doi.org/10.1186/s13195-024-01458-z.
[35] Pereira JB, Janelidze S, Smith R, Mattsson-Carlgren N, Palmqvist S, Teunissen CE, et al. Plasma GFAP is an early marker of amyloid-β but not tau pathology in Alzheimer's disease. Brain 2021;144:3505–16. https://doi.org/10.1093/brain/awab223.
[36] Cui L, Tu Y-Y, Zhang Z, Guo Y-H, Guan Y-H, Xie F, et al. Associations and potential multiple mechanisms between subjective hearing loss and cognitive impairment. J Prev Alzheimers Dis 2024;11:649–60. https://doi.org/10.14283/jpad.2024.62.
[37] Huang Y, Huang L, Wang Y, Liu Y, Lo C, Guo Q. Differential associations of visual memory with hippocampal subfields in subjective cognitive decline and amnestic mild cognitive impairment. BMC Geriatr 2022;22:153. https://doi.org/10.1186/s12877-022-02853-7.
[38] Gollan TH, Garcia DL, Stasenko A, Murillo M, Kim C, Galasko D, et al. The MINT Sprint 2.0: a picture naming test for detection of naming impairments in Alzheimer's disease and in preclinical AD. Alzheimers Dement 2024;20:112–23. https://doi.org/10.1002/alz.13381.
[39] Zhang Z, Cui L, Huang L, Guan Y-H, Xie F, Guo Q-H. Development and validation of the Chinese Naming Test (CNT): diagnostic efficacy and correlation with Alzheimer's disease biomarkers. J Alzheimers Dis 2025;104:1259–69. https://doi.org/10.1177/13872877251324100.
[40] Garcia Condado J, Cortes JM. Alzheimer's Disease Neuroimaging Initiative. NeuropsychBrainAge: a biomarker for conversion from mild cognitive impairment to Alzheimer's disease. Alzheimers Dement (Amst) 2023;15:e12493. https://doi.org/10.1002/dad2.12493.
[41] Yin C, Imms P, Cheng M, Amgalan A, Chowdhury NF, Massett RJ, et al. Anatomically interpretable deep learning of brain age captures domain-specific cognitive impairment. Proc Natl Acad Sci U S A 2023;120:e2214634120. https://doi.org/10.1073/pnas.2214634120.
[42] Taylor A, Zhang F, Niu X, Heywood A, Stocks J, Feng G, et al. Investigating the temporal pattern of neuroimaging-based brain age estimation as a biomarker for Alzheimer's Disease related neurodegeneration. Neuroimage 2022;263:119621. https://doi.org/10.1016/j.neuroimage.2022.119621.
[43] Chafee MV, Heilbronner SR. Prefrontal cortex. Curr Biol 2022;32:R346–51. https://doi.org/10.1016/j.cub.2022.02.071.
[44] Schwartenbeck P, Baram A, Liu Y, Mark S, Muller T, Dolan R, et al. Generative replay underlies compositional inference in the hippocampal-prefrontal circuit. Cell 2023;186:4885–97. https://doi.org/10.1016/j.cell.2023.09.004. .e14.
[45] Park AJ, Harris AZ, Martyniuk KM, Chang C-Y, Abbas AI, Lowes DC, et al. Reset of hippocampal-prefrontal circuitry facilitates learning. Nature 2021;591:615–9. https://doi.org/10.1038/s41586-021-03272-1.
[46] Brown TI, Rissman J, Chow TE, Uncapher MR, Wagner AD. Differential medial temporal lobe and parietal cortical contributions to real-world autobiographical episodic and autobiographical semantic memory. Sci Rep 2018;8:6190. https://doi.org/10.1038/s41598-018-24549-y.
[47] Wei L, Zhang Y, Wang J, Xu L, Yang K, Lv X, et al. Parietal-hippocampal rTMS improves cognitive function in Alzheimer's disease and increases dynamic functional connectivity of default mode network. Psychiatry Res 2022;315:114721. https://doi.org/10.1016/j.psychres.2022.114721.
[48] Banks SJ, Zhuang X, Bayram E, Bird C, Cordes D, Caldwell JZK, et al. Default mode network lateralization and memory in healthy aging and Alzheimer's disease. J Alzheimers Dis 2018;66:1223–34. https://doi.org/10.3233/JAD-180541.
[49] Ushakov V, Sharaev MG, Kartashov SI, Zavyalova VV, Verkhlyutov VM, Velichkovsky BM. Dynamic causal modeling of hippocampal links within the Human default mode network: lateralization and computational stability of effective connections. Front Hum Neurosci 2016;10:528. https://doi.org/10.3389/fnhum.2016.00528.
[50] Liu H, Li Y, Sun Z, Xu X, Yan B, Li Y, et al. Altered hemispheres lateralization of brain functional gradients in Alzheimer's disease. J Alzheimers Dis 2025:13872877251339761. https://doi.org/10.1177/13872877251339761.
[51] Westlye ET, Lundervold A, Rootwelt H, Lundervold AJ, Westlye LT. Increased hippocampal default mode synchronization during rest in middle-aged and elderly APOE ε4 carriers: relationships with memory performance. J Neurosci 2011;31:7775–83. https://doi.org/10.1523/JNEUROSCI.1230-11.2011.
[52] Grajski KA, Bressler SL. Alzheimer's Disease Neuroimaging Initiative. Differential medial temporal lobe and default-mode network functional connectivity and morphometric changes in Alzheimer's disease. Neuroimage Clin 2019;23:101860. https://doi.org/10.1016/j.nicl.2019.101860.
[53] Jiménez-Balado J, Eich TS. GABAergic dysfunction, neural network hyperactivity and memory impairments in human aging and Alzheimer's disease. Semin Cell Dev Biol 2021;116:146–59. https://doi.org/10.1016/j.semcdb.2021.01.005.
[54] Dillen KNH, Jacobs HIL, Kukolja J, Richter N, von Reutern B, Onur ÖA, et al. Functional disintegration of the default mode network in prodromal Alzheimer's disease. J Alzheimers Dis 2017;59:169–87. https://doi.org/10.3233/JAD-161120.
[55] Tripathi V, Batta I, Zamani A, Atad DA, Sheth SKS, Zhang J, et al. Default mode network functional connectivity As a transdiagnostic biomarker of cognitive function. Biol Psychiatry Cogn Neurosci Neuroimaging 2025;10:359–68. https://doi.org/10.1016/j.bpsc.2024.12.016.
[56] Corriveau-Lecavalier N, Gunter JL, Kamykowski M, Dicks E, Botha H, Kremers WK, et al. Default mode network failure and neurodegeneration across aging and amnestic and dysexecutive Alzheimer's disease. Brain Commun 2023;5:fcad058. https://doi.org/10.1093/braincomms/fcad058.